HHS Public Access

Author manuscript

Nucl Med Biol. Author manuscript; available in PMC 2019 July 01.

Published in final edited form as:

Nucl Med Biol. 2018 ; 62-63: 63–70. doi:10.1016/j.nucmedbio.2018.05.004.

One-Pot Synthesis and Bio-distribution of Fluorine-18 Labelled Serum Albumin for Vascular Imaging

Falguni Basuli[1,*], **Xiang Zhang**[1], **Mark R. Williams**[2], **Jurgen Seidel**[2,3], **Michael V. Green**[2,3], **Peter L. Choyke**[2], **Rolf E. Swenson**[1], and **Elaine M. Jagoda**[2]

[1]Imaging Probe Development Center, National Heart, Lung, and Blood Institute, National Institutes of Health, Rockville, MD

[2]Molecular Imaging Program, National Cancer Institute, National Institutes of Health, Bethesda, MD

[3]Contractor to Leidos Biomedical Research, Inc. (formerly SAIC-Frederick, Inc.), NCI-Frederick, Frederick, Maryland, 21702, United States

Abstract

Introduction: Equilibrium single-photon radionuclide imaging methods for assessing cardiac function and the integrity of the vascular system have long been in use for both clinical and research purposes. However, positron-emitting blood pool agents that could provide PET equivalents to these (and other) clinical procedures have not yet been adopted despite technical imaging advantages offered by PET. Our goal was to develop a PET blood pool tracer that not only meets necessary *in vivo* biological requirements but can be produced with an uncomplicated and rapid synthesis method which would facilitate clinical translation. Herein, albumin labeled with fluorine-18 was synthesized using a one-pot method and evaluated *in vitro* and *in vivo* in rats.

Methods: A ligand (NODA-Bz-TFPE), containing NODA attached to a tetrafluorophenylester (TFPE) via a phenyl linker (Bz), was labeled with aluminum fluoride (Al[^{18}F]F). Conjugation of the serum albumin with the ligand (Al[^{18}F]F-NODA-Bz-TFPE), followed by purification (size exclusion chromatography), yielded the final product (Al[^{18}F]F-NODA-Bz-RSA/HSA). *In vitro* stability was evaluated in human serum albumin by HPLC. Rat bio-distributions and whole-body PET imaging over a 4h time course were used for the *in vivo* evaluation.

Results: This synthesis exhibited an overall radiochemical yield of 45 ± 10% (n = 30), a 50-min radiolabeling time, a radiochemical purity > 99% and apparent stability up to 4 h in human serum. Blood had the highest retention of Al[^{18}F]F-NODA-Bz-RSA at all times with a blood half-life of 5.2 h in rats. Al[^{18}F]F-NODA-Bz-RSA distribution in most rat tissues remained relatively constant for up to 1 h, indicating that the tissue radioactivity content represents the respective tissue plasma volume. Dynamic whole-body PET images were in agreement with these findings.

[*]Corresponding Author.

Conclusions: A new ligand has been developed and radiolabeled with Al[^{18}F]F that allows rapid (50-min) preparation of fluorine-18 serum albumin in one-pot. In addition to increased synthetic efficiency, the construct appears to be metabolically stable in rats. This method could encourage wider use of PET to quantify cardiac function and tissue vascular integrity in both research and clinical settings.

1. Introduction

Radionuclide procedures based on imaging the equilibrium distribution of a radiotracer distributed uniformly throughout the blood pool have proven extremely useful in both clinical and research settings [1-6]. Depending on the specific properties of the agent, procedures have been devised that include locating sites of regional hemorrhage [7-8], assessing vascular permeability in cancerous tissues [9], identifying sites of tissue leakage and inflammation in response to traumatic injury [10] and, commonly, visualization and quantification of cardiac left ventricular function in patients with heart disease [11, 12] and those undergoing cancer chemotherapy with drugs that compromise cardiac function [13, 14].

Today, most of these imaging procedures are carried out with gamma camera-based SPECT imaging systems and single-photon labeled tracers, e.g. ^{99m}Tc-labeled red blood cells. In contrast, routine clinical blood pool imaging with PET is uncommon which in most likely a consequence of the lack of a comparable, clinically approved PET agent. Nonetheless, equilibrium PET imaging of the vascular system offers several compelling advantages over single photon methods, particularly if the radiolabel is fluorine-18 (because of its nuclear and chemical properties). It is not surprising, therefore, that a variety of fluorine-18 labeled prosthetic groups have been used to radiolabel human (HSA) and rat (RSA) serum albumin, e.g. 2,3,5,6-tetrafluorophenyl penta-[^{18}F]fluorobenzoate [15], 4-nitrophenyl-2-[^{18}F]fluoropropionate [16], methyl 3-[^{18}F]fluoro-5-nitrobenzimidate [17], 4-[^{18}F]fluorophenacylbromide [17],4-azidophenacyl-[^{18}Flfluoride ([^{18}F]APF) [16], [^{18}F]fluorobenzaldehyde ([^{18}F]FBA) [18], [^{18}F]SFB [16], ^{18}F-labelled sulfonamide-based click chemistry building blocks [19] and a Si[^{18}F]F bonded prosthetic groups [20, 21]. However, the radiolabeled products resulting from these methods exhibit differences in *in vivo* bio-distribution properties that most likely result from conditions prevailing during synthesis or alterations in metabolism due to differences between prosthetic groups and their linkage to the protein [9, 21, 22].

We have previously reported the synthesis of fluorine-18 labeled albumin ([^{18}F]F-NE-HSA/RSA, Figure 1) [23] in a 90-min synthesis, using Olberg's ligand [^{18}F]fluoronicotinate ([^{18}F]F-NE) [24], that has favorable biodistribution properties. This agent remains in the blood pool for an extended period of time compared to other serum proteins (i.e. transferrin) and accumulates slowly in the tissues of the major body organ (with the exception of the kidneys). As a result, this compound can be used in applications that include measurement of physical specific organ plasma volume (the physical plasma volume of blood in the organ per unit mass of organ tissue), visualizaton and quantification of cardiac function by ECG-gated imaging of the heart, and measurement of specific organ plasma distribution volumes to assess vascular "leakage" in cancerous and inflamed tissues. Importantly, this

radiolabeled albumin exhibited stable tissue distributions over 4 h indicating that this agent could be used to make multiple tissue plasma volume measurements over time periods several hours long to assess the effects of interventions, an experimentally useful paradigm.

We sought to investigate an alternative procedure to radiolabel serum albumin (HSA/RSA) using an Al[^{18}F]F chelate, with the intention of shortening and simplifying the synthetic process while retaining the advantageous properties of the [^{18}F]F-NE-RSA/HSA compound. McBride et al. were the first to demonstrate the use of a one step AlF method to radiolabel biomolecules with high molar activity [25]. Among all the ligands tested, the pentadentate ligand, 1,4,7-triazacyclononane-1,4-diacetic acid (NODA) [26-28] was the preferred ligand for the Al[^{18}F]F method. In this labeling method, chelation of Al[^{18}F]F with NODA was achieved at elevated temperature (100 °C) in one step. This condition is not suitable for proteins since most proteins are unstable at this temperature. McBride et al. have also reported a two-step indirect method for labeling of temperature sensitive biomolecules [28] based on labeled maleimide conjugation with a thiol functionality of protein. Other groups have subsequently adopted this method (one step/two-step) to radiolabel a variety of biomolecules [29-34]. In this work, we report a new ligand (NODA-Bz-TFPE) for conjugation with amine functionalities of protein to synthesize fluorine-18 labeled albumin and compare the bio-distribution properties of this agent to those observed in our previous work [23] and to other literature compounds [18, 21]. This method was based on the synthesis of a NODA ligand functionalized with tetrafluorophenyl ester (NODA-Bz-TFPE) followed by labeling of the ligand with Al[^{18}F]F. The labeled ligand was then conjugated to the amine functionalities of albumin and purified by size exclusion chromatography using a mini-Trap column to produce the final labeled albumin product which was then evaluated *in vitro* and *in vivo*.

2. Materials and Methods

Di-tert-butyl 2,2'-(1,4,7-triazonane-1,4-diyl)diacetate was purchased from CheMatech, France (Dijon, France) and used as received. Whole human serum was obtained from MP Biomedicals, LLC (Solon, OH, USA). Fluorine-18 was received from National Institutes of Health cyclotron facility (Bethesda, MD, USA). Phosphate-buffered saline (PBS) 1X (12 mM phosphate buffer, pH 7.4, 137 mM NaCl, and 2.7 mM KCl) was obtained from Life Technologies (Carlsbad, CA, USA). All other chemicals and solvents were received from Sigma Aldrich (St. Louis, MO, USA) and used without further purification. PD10 MiniTrap™ columns were obtained from GE Healthcare Bioscience (Pittsburg, PA, USA). Chromafix 30-PS-HCO_3 anion-exchange cartridge was purchased from Macherey-Nagel (Düren, Germany) and used as received. Other columns, the Sep-Pak® cartridges and the iTLC-SG plates used in this synthesis were obtained from Agilent Technologies (Santa Clara, CA, USA) and Waters (Milford, MA, USA), respectively. Mass spectrometry (MS) was performed on a 6130 Quadrupole LC/MS, Agilent Technologies instrument equipped with a diode array detector. ^{1}H, ^{13}C and ^{19}F NMR spectra were recorded on a Varian spectrometer (400 MHz). Chemical shifts (ppm) are reported relative to the solvent residual peaks of acetonitrile (δ ^{1}H, 2.50 ppm; ^{13}C 118.26, 1.79). ^{19}F NMR spectra are reported with reference to the trifluoracetic acid (δ ^{19}F, −76.72 ppm). High-resolution mass spectra were recorded on an ESI-TOF. HPLC purification and analytical HPLC analysis were performed

on an Agilent 1200 Series instrument equipped with multi-wavelength detectors along with a flow count radiodetector (Eckert & Ziegler, B-FC-3500 diode). iTLC-SG papers were developed using a mixture of acetonitrile and water (3:1, v/v). The papers were read in an Eckert & Ziegler TLC scanner (B-AR2000-1)

HPLC conditions:

Method A; Column : Agilent XDB C18 column (9.4 × 250 mm, 5 μm). Mobile phase: A: water (0.1% TFA); B: acetonitrile (0.1% TFA). Gradient: 40 - 57% B in 7-min; flow rate of 4 mL/min. Method B; Column : Agilent XDB C18 column (4.6 × 150 mm, 5 μm). Mobile phase: A: water (0.1% TFA); B: acetonitrile (0.1% TFA). Gradient: 5 - 70% B in 15-min; flow rate of 1 mL/min. Method C; Column : Agilent Eclipse GF 250, 5 μm, 4.6 × 250 mm column, PBS buffer (pH 7.4), flowrate: 1 ml/min.

2.1 Synthesis of ligand

2.1.1. ***Synthesis of 4-((4,7-bis(2-(tert-butoxy)-2-oxoethyl)-1,4,7-triazonan-1-yl)methyl)benzoic acid*** **(Scheme 1: compound 2)—**To the solution of di-tert-butyl 2,2'-(1,4,7-triazonane-1,4-diyl)diacetate (**1**, 500 mg, 1.4 mmol) in anhydrous dichloromethane (20 ml) was added 200 μL of triethylamine (1.4 mmol) followed by 4-(bromomethyl)benzoic acid (310 mg, 1.4 mmol) in 5 mL anhydrous dichloromethane. The mixture was stirred at room temperature for 24 h. The mixture was washed with water, dried over sodium sulfate. The solvent was evaporated to produce the crude product and recrystallized from acetonitrile and diethyl ether to obtain 4-((4,7-bis(2-(tert-butoxy)-2-oxoethyl)-1,4,7-triazonan-1-yl)methyl)benzoic acid (**2,** 586 mg, 1.2 mmol, 86%) as a white solid.

^{1}H NMR (400 MHz, Acetonitrile-d_3) δ 8.00 (d, J = 7.9 Hz, 2H), 7.68 (d, J = 8.0 Hz, 2H), 4.51 (s, 2H), 3.50 – 3.02 (m, 10H), 2.96 – 2.67 (m, 6H), 1.43 (s, 18H). ^{13}C NMR (101 MHz, CD_3CN) δ 170.36, 166.46, 136.92, 132.24, 130.48, 130.02, 81.34, 58.22, 55.89, 50.89, 49.95, 47.55, 27.46. MS (ESI) calculated mass for the parent $C_{26}H_{41}N_3O_6$, 492.31 $[M + H]^+$, found 492.30 $[M + H]^+$.

2.1.2. ***Synthesis of 2,2'-(7-(4-((2,3,5,6-tetrafluorophenoxy)carbonyl)benzyl)-1,4,7-triazonane-1,4-diyl)diacetic acid*** **(NODA-Bz-TFPE, Scheme 2)—**To the solution of **2** (586 mg, 1.2 mmol) in dioxane (30 mL) was added dicyclohexyl carbodiimide (DCC) (240 mg, 1.2 mmol) followed by 2,3,5,6-tetrafluorophenol (200 mg, 1.2 mmol). The mixture was stirred for 24 h and filtered. Solvent was evaporated under reduced pressure to produce di-tert-butyl 2,2'-(7-(4-((2,3,5,6-tetrafluorophenoxy)carbonyl)benzyl)-l,4,7-triazonane-1,4-diyl)diacetate (**3**). To the dichloromethane (5 mL) residue, 5 mL of trifluoroacetic acid was added. The solution was stirred at room temperature for 24 h and the solvent was removed under reduced pressure. The final product was purified by semi-prep HPLC to produce pure 2,2'-(7-(4-((2,3,5,6-tetrafluorophenoxy)carbonyl)benzyl)-1,4,7-triazonane-1,4-diyl)diacetic acid (NODA-Bz-TFPE, 317 mg, 0.6 mmol, 50%).

^{1}H NMR (400 MHz, CD_3CN) 8.25 (d, J = 8.3 Hz, 2H), 7.75 (d, J = 8.3 Hz, 2 H), 7 .40 (tt, J = 10.5, 7.2 Hz, 1H), 4.34 (s, 2H), 3.74 – 3.31 (m, 4H), 3.21 – 2.6 4 (m, 12H); ^{13}C NMR (101 MHz, CD_3CN) δ 171.24, 162.28, 159.49 (m), 146.13 (d, J = 246 Hz), 140.95, 140.85 (d, J = 249 Hz), 130.96 (m), 130.81, 127.29, 103.98, 58.48, 54.63, 50.01, 49.34, 47.97; ^{19}F NMR ($CDC1_3$, 100 MHz): δ −140.95 (m), −154.80 (m). HRMS (ESI-TOF) calculated mass for the parent compound $C_{24}H_{25}F_4N_3O_6$, 528.1752 $[M + H]^+$, found 528.1758 $[M + H]^+$.

2.2 Radiolabeling

2.2.1. *Synthesis of Al[^{18}F]F-NODA-Bz-TFPE and (*(Al[^{18}F]F-NODA-Bz-RSA, Scheme 2*)*—

Fluorine-18 containing target water was either directly used or purified by an anion-exchange cartridge (30-PS-HCO_3). For purification, fluorine-18 trapped on the (30-PS-HCO_3) cartridge was washed with water (3 mL) and fluorine-18 was eluted with saline (400 μL). To the mixture of NODA-Bz-TFPE in DMSO (50 μL, 32 μg, 60 nmol) and $AlCl_3$ (4.0 μg, 1.5mM, 30 nmol) in 0.5 M sodium acetate (pH 5) was added fluorine-18 (50-200 μl, 50-200 mCi, 1.85-7.4 GBq) and heated at 100 °C for 15-min. The final pH of the solution was ~4.5. The reaction mixture was cooled to ambient temperature. Albumin (RSA or HSA, 20 mg) was dissolved in 150 μL of 0.2 M phosphate buffer (pH 10). The pH of the solution was adjusted to 8 by adding 100 μL of 0.5 M phosphate buffer (pH 10). This albumin solution was added to the solution of Al[^{18}F]F-NODA-Bz-TFPE and incubated at 40 °C for 15-min. The product was purified by size exclusion chromatography (column: PD10 Minitrap) using PBS as an eluent. The final product (Al[^{18}F]F-NODA-Bz-RSA/HSA-AIF, 45± 10%, ≥ 99% radiochemically pure) was collected in 0.8 mL of phosphate buffer.

2.3. In vitro serum stability

To test serum stability, 14 mCi (518 MBq) of (Al[^{18}F]F-NODA-Bz-RSA in 300 μL of PBS (1X, pH 7.4) was added to whole human serum (2 mL) kept at 37 °C for up to 4 h during which radiochemical purity was monitored by size exclusion HPLC.

2.4. Rat Biodistribution Studies

Rats [male, 6 to 8 weeks (127.11 ± 17.2 g), Fischer 344 (#403), Charles River Laboratories, Wilmington, MA)] were injected via tail vein (50 to 100 μCi; 1.85 to 3.7 MBq per rat) with Al[^{18}F]F-NODA-Bz-RSA and after an awake period of 0.5, 1, 2 or 4 h post injection, were euthanized, blood and tissues were excised, weighed and their radioactivity content determined by gamma counting (Perkin Elmer 2480 Wizard 3). Measurements of radioactivity in digestive tract tissues, e.g. small intestines, included the contents of these tissues.

Tissue and blood radioactivity amounts, expressed as differential uptake ratio (DUR): [(%injected dose/tissue (g)) x (body weight (g))]/100, and the ratios of these quantities, T:B, were determined for various organs (see Appendix).

Statistical analysis was performed using a Welch's t test (GraphPad InStat version 3.00 for Windows, GraphPad Software, San Diego California USA).

Animal Care: NCI-Frederick is accredited by AAALAC International and follows the Public Health Service Policy for the Care and Use of Laboratory Animals. Animal care was provided in accordance with the procedures outlined in the "Guide for Care and Use of Laboratory Animals" (National Research Council; 1996; National Academy Press; Washington, D.C.).

2.5. PET Imaging Studies

Whole body (WB) imaging was performed on rats (Fischer SAS #403/Charles River, mean weight 169 ± 2 g) anesthetized with an isoflurane/O_2 mixture (1.5-2.0% v/v) on the bench top and injected via tail with Al[^{18}F]F-NODA-Bz-RSA (607 ± 41 μCi; 22.5 ± 1.5 MBq;). Each animal was then transferred to the pre-heated scanning bed of the BioPET/CT (Sedecal, Madrid, Spain., evaluated as the GE eXplore Vista) [35] and exposed to the same isoflurane/oxygen mixture throughout the 160-min scanning period.

The scanner was set to acquire four consecutive WB scans starting 30-min post injection. Each WB scan was comprised of four bed positions at 10-min/position for a single WB scanning time of 40-min. The first bed position visualized the head and shoulders of the rat while the fourth bed position visualized the abdomen, bladder, etc. These dynamic WB imaging data were reconstructed (2 iterations, 20 subsets) with the 3DOSEM resolution recovery algorithm [36] available on the BioPET/CT and decay corrected to the start time of WB imaging in that animal. Maximum intensity projection images of each WB scan were created to qualitatively assess the time variation of Al[^{18}F]F-NODA-Bz-RSA in each animal and to allow comparison of these changes across rats.

3. Results

3. 1. Chemistry, Radiochemistry and In Vitro Serum Stability

Synthesis of the NODA-Bz-TFPE is outlined in Scheme 1. The syntheses were performed in three steps. The alkylation of commercially available compound **1** with 4-(bromomethyl)benzoic acid afforded intermediate **2** in 86% yield. Tetrafluorophenyl ester formation of intermediate **2** using 2,3,5,6-tetrafluorophenol and a coupling agent DCC was achieved in anhydrous dioxane. Deprotection of t-Bu group with trifluoroacetic acid produced the final ligand which was purified by semi-prep HPLC with 50% yield. Extensive studies have already been performed to find the optimum pH, temperature, mole ratio, solvents etc. [26-28] for effective chelation and based on those studies fluorine-18 labeling of the NODA-Bz-TFPE ligand was performed at 100 °C for 15-min (Scheme 2). Formation of the Al[^{18}F]F-NODA-Bz-TFPE was checked by analytical HPLC (Figure 2). The radiochemical conversion (93 ± 5%, n = 3) was determined by iTLC. Radiochemical yield was unchanged whether the fluorine-18 containing target water was used directly or after purification by passing through an anion exchange cartridge (PS-HCO_3) [32, 37]. Conjugation of Al[^{18}F]F-NODA-Bz-TFPE with RSA was performed at 40 °C for 15-min at pH 8. Labeled albumin was purified by size exclusion chromatography using a PD10 Minitrap size exclusion column using PBS (pH 7.4) as an eluent. This size exclusion column completely removed fluorine-18/[^{18}F]AlF and unreacted chelate (Figure 3a) from the final product (Figure 3b). The overall radiochemical yield was 45 ± 10 % (n = 30) in a 50-min

synthesis, with a radiochemical purity ≥ 99%. In a typical reaction, starting with 3.7 GBq of fluorine-18, we obtained 1.4 GBq of product with a molar activity of 8000 MBq/μmol. Since one of the goals of this study was to develop a facile methodology for preparing fluorine-18 labeled albumin for clinical vascular imaging, the conjugation reaction was also tested with human serum albumin (HSA). The overall radiochemical yield (45 ± 9.7 %, n = 10) was comparable with RSA labeling. The labeled albumin (RSA) was stable up to 4 h in whole human serum (Figure S1).

3.2. Rat Biodistribution Studies

Blood had the highest retention of Al[^{18}F]F-NODA-Bz-RSA (Figure 4A) at all times with DURs of 13.2, 11.4, 9.2, and 8.1 at 0.5 h, lh, 2 h and 4 h. The next highest Al[^{18}F]F-NODA-Bz-RSA retentions were observed in the lungs (DURs: 4.8 to 3.6; $P < 0.001$; n=5 per group), heart (DURs: 3.6 to 2.9; $P < 0.001$; n=5 per group), and kidneys (DURs: 3.3 to 4.6; $P < 0.001$; n=5) which were significantly decreased by 1.8 to 4.0-fold compared to blood DURs at the same times. Similarly, significant decreases in radioactive content ranging from 3.5 to 7.1-fold were observed in the DURs of liver (DURs: 2.7 to 2.3; $P < 0.001$; n=5 per group) and spleen (DURs 1.8 to 2.0; $P < 0.001$; n=5 per group) compared to the blood DURs at the same times. DURs of the small intestine and pancreas were decreased further (6.4 to 17.8-fold) compared to blood DURs at the same times with colon, stomach and muscle exhibiting the lowest DURs (decreased by 63.4 to 15.0-fold). Femur DURs (1.3 to 1.0) over the time course exhibited little change suggesting minimal de-fluorination of Al[^{18}F]F-NODA-Bz-RSA or accumulation of other bone-seeking breakdown products. The blood half life, $t_{1/2}$, calculated from the blood DURs over the study period, was 5.2 h (one component exponential equation: $y = 13.21369\ e^{-0.00221x}$; $R^2 = 0.90$).

Although the ratios of tissue to blood DURs (Figure 4B) generally increased with time for all tissues, the T:B ratios from 0.5 h to 1 h of the lung, heart, liver, spleen, muscle, colon, femur, stomach and pancreas remained relatively constant with no significant differences (Table 1) during this interval ($P > 0.05$; n= 5 per group), whereas 2 h and beyond, all T:B ratios (except the heart at 2 h) were significantly increased ($P < 0.05$; n= 5 per group; also see Appendix). Since the T:B ratios are proportional to the specific plasma distribution volume (ml of plasma/gm of tissue) in these tissues, these early ratios are likely proportional to the physical specific plasma volume of these organs, implying that the tissue/organ vasculature is intact and that Al[^{18}F]F-NODA-B-RSA has not leaked into the tissue or been metabolized in appreciable amounts. The statistical significance of the changes (%) observed in the T:B ratios from 0.5 h to 1 h , 0.5 h to 2 h and 0.5 to 4h are listed in Table 1. The greatest increases in T:B ratios were observed from 0.5 h to 4 h in the colon (219%), muscle (169%), kidney (128%), spleen (78%) and small intestine (77%). The significant increases in T:B ratios in the hepatobiliary system, gastrointestinal tract and kidneys at the later time points indicates the presence of metabolic products of Al[^{18}F]F-NODA-Bz-RSA. As a result, T:B ratios in these organs are not proportional to their physical specific blood volumes at these times but instead represent the specific distribution volumes of the agent and it's radiolabeled metabolites in these organs/tissues.

3.3 PET Imaging Studies

A representative WB dynamic image of one rat is shown in Figure 5. As expected, the central vasculature, e.g. the cardiac ventricular chambers, and vasculature of the major organs, e.g. lungs, liver, spleen, are well visualized throughout the study. Activity is also distinguishable in the cortex and medulla of both kidneys in all four of the rat images. Activity is also present in the bladder in all scans and changes slowly with time. Note particularly the changing distribution of activity in the bowel throughout the study, an effect present in all animals. There was no apparent concentration of activity in the skeleton that could not be attributed to local blood volume suggesting that bone-seeking breakdown products, e.g. free fluoride, other metabolites, are not present in significant amounts.

4. Discussion

Recently we reported fluorine-18 labeling of serum albumin using Olberg's ligand ([^{18}F]F-NE) and this radiolabeled albumin exhibited excellent blood pool imaging properties [23, 24]. In this work, we sought to further simplify the method by using an AlF method reported by McBride's group [28]. For this study, we wanted to prepare a ligand which would have 1,4,7-triazacyclononane-1,4-diacetate (NODA) attached with a tetrafluorophenyl ester via a phenyl linker since it has already been proven that NODA is a good chelator for aluminum [26-28] and the tetrafluorophenyl ester is an efficient functional group for conjugation with amine groups at higher pHs [38]. This one-pot radiolabeling method requires two steps. The first step is the formation of Al[^{18}F]F-NODA-Bz-TFPE chelate (Scheme 2) and the second step is the conjugation with rat serum albumin. The direct consequence of this labeling approach is a significant reduction in synthesis time from about 90-min for the previously reported NE method [23] to about 50-min with this AlF method.

An implicit assumption underlying this labeling approach is that the resulting product will also possess favorable imaging properties similar to those found in our earlier work [23]. The tissue:blood bio-distributions of [^{18}F]F-NE-RSA and Al[^{18}F]F-NODA-Bz-RSA are directly compared in Figure 6. Two features present in this comparison are noteworthy. First, after the first hour, almost all tissue to blood ratios for Al[^{18}F]F-NODA-Bz-RSA are significantly increased ($P << 0.05$, 2h and 4 h, Table 1) relative to the 30-min values. In contrast, only after 4 h do kidney, muscle and femur tissue to blood ratios for [^{18}F]F-NE-RSA differ significantly from the 30-min values [23]. This result suggests that the Al[^{18}F]F-NODA-Bz-RSA compound is best suited to imaging procedures that require an hour or less to complete in rats, particularly physical organ plasma volume measurements. After this time, this compound, and most others described in the literature, become increasingly restricted to ECG-gated cardiac function measurements where falling blood and increasing organ activities do not significantly comprise these measurements.

A second result is also evident in Figure 6. Since imaging measurements of specific organ plasma volumes (see Appendix) are a possible application for these compounds, values obtained for these volumes in this and other studies should generally agree with those reported in the literature [39]. A survey of the literature, however, reveals a very wide range of specific organ plasma volumes in rats (differing for the same organ by a factor of two or more in some cases). This finding suggests that organ plasma volume determinations may

vary depending on the measurement method, experimental design and rat strain used to determine tissue plasma volumes. While methods of measuring organ plasma volume with fluorine-18 labeled albumin may have their own biases, the results portrayed in Figure 6 are from two independent studies performed with different groups of animals injected with either [^{18}F]F-NE-RSA or Al[^{18}F]F-NODA-Bz-RSA. Despite these differences, tissue to blood ratios for both products are virtually identical at the earliest time point as would be expected if both are measuring the same physical entity, i.e. physical organ plasma volume. These results support, though do not prove, the hypothesis that organ plasma volume measurements with these products do yield a valid estimate of these volumes if carried out before significant tissue uptake occurs.

Finally, recently reported methods for labeling albumins [9, 21, 40] also exhibit different time dependent variations in organ radioactivity levels and thus these methods are also application dependent. The novel *in vivo* albumin labeling method described by Ni, et al. is illustrative of the tradeoff between ease of synthesis and the resulting alteration in bio-distribution properties [9]. For this novel *in vivo* method, Evans blue was labeled with fluorine-18 in 30-min and then injected into mice thereby labeling endogenous albumin *in vivo*. In addition, fluorine-18 labeled Evans blue conjugated to albumin was synthesized *in vitro* and injected into mice to determine its biodistribution. The bio-distribution of these two agents, though grossly similar, differed in detail. Following *in vivo* labeling in mice, liver and blood activities began to immediately decline whereas for the *in vitro* compound, blood and liver activities changed little during the first third (about 20-min) of the overall observation period and declined more slowly thereafter. These results suggest that the compound developed by Niu, et al. may be best suited for plasma volume measurements made shortly after injection and for cardiac function studies at both early and later times. The bio-distributions of the [^{18}F]F-NE-RSA and Al[^{18}F]F-NODA-Bz-RSA compounds compared here suggest a similar strategy, i.e. that both preparations can yield reliable measurements of physical tissue plasma volumes in rats if carried out within an hour or so post-administration, but if physical specific plasma volume measurements are required at later times, the [^{18}F]F-NE-RSA compound would be the better choice since tissue accumulation of this agent is much lower over time (Figure 6). It is important to note that in the case of clinical applications, the time available for reliable measurements of all kinds would be expected to be substantially longer due to the lower metabolic rate of human subjects. Both preparations, however, would be suitable for ECG-gated cardiac imaging at almost any reasonable time post-injection.

5. Conclusion

We have synthesized a new ligand for simplified radiolabeling of RSA with Al[^{18}F]F. A radiochemical yield of 45 ± 10% (n = 30) was obtained with a 50-min synthesis. This method yields a PET vascular imaging agent that, with some temporal limitations, is suitable for quantifying phenomena such as the specific physical and distribution volumes of plasma in normal and cancerous tissues and cardiac function in both animals and man. This simplified and time-efficient method may thus encourage PET blood pool imaging in both clinical and research settings.

Supplementary Material

Refer to Web version on PubMed Central for supplementary material.

Acknowledgments

Financial support: This project has been funded in whole or in part with federal funds from the National Cancer Institute, National Institutes of Health, under contract HHSN261200800001E. The content of this publication does not necessarily reflect the views or policies of the Department of Health and Human Services, nor does mention of trade names, commercial products, or organizations imply endorsement by the U.S. Government. This research was supported [in part] by the Intramural Research Program of the NIH, National Cancer Institute, Center for Cancer Research.

Appendix:

Tissue to Blood Ratios of fluorine-18 labeled albumin as a Measure of Specific Organ Plasma Distribution Volume

The differential uptake ratio (DUR) for each tissue was determined at each time point from the bio-distribution measurements:

$$\text{DUR} = [\%\text{injected dose}/(\text{g of tissue}/\text{g body weight})]/(100)$$

If D is the injected dose in MBq, A is the activity in the tissue (MBq), W_T is the tissue weight and W is the body weight in grams, then:

$$\text{DUR} = [(100\ A/D)/(W_T/\ W)]/100$$

If the well counter count rate for the tissue and injected dose are R_T and R_D, respectively, and k is the proportionality constant that converts count rate to MBq, then:

$$R_T = kA \text{ and } R_D = kD$$

and:

$$\text{DUR} = [(R_T/R_D)/\ (W_T/\ W)]/100 \quad [1]$$

The tumor to blood ratio (T:B) used in this work is the ratio of the tissue (T) and blood (B) DURs:

$$\text{T:B} = \text{DUR}_T\ /\text{DUR}_B = [(R_T/R_D)_T/(W_T/\ W)]/[(R_B/R_D)_B/\ (W_B/\ W)] \quad \text{or,}$$

$$\text{T:B} = (R_T\ /W_T)/(R_B/W_B)$$

Shortly after administration, the plasma concentration of albumin blood labels such as [^{18}F]AlF-NODA-Bz-RSA becomes uniform throughout the blood pool and declines slowly with time. If the count rate of a sample of this plasma is R_p and, at the same moment, the total count rate from an entire organ containing the agent is R_T, then the specific distribution volume of plasma in that organ (ml/g of tissue) is given by:

$$V_P\ (\text{ml/g}) = [R_T / W_T\ ] / [R_P / (W_P / \rho_P)] \quad [2]$$

where R_p is the count rate from the plasma fraction of a sample drawn from some convenient location in the vascular system (here, the arterial system) and counted at the same time as the whole organ, ρ_p is the physical density of the plasma sample and W_p is the weight of that plasma sample.

In the present work, a whole blood sample rather than a plasma sample was counted. Since $R_P/(W_P/\rho_P) = \rho_B(R_B/W_B)/(1\text{-}H_B)$ where R_B is the count rate of whole blood, ρ_B is the density of whole blood, W_B is the weight of the whold blood sample and H_B is the hematocrit of the blood sample, Eqn. 2 becomes:

$$V_P\ (\text{ml/g}) = [(R_T/W_T)/[\rho_B(R_B/W_B)/(1 - H_B)] = (T{:}B)(1 - H_B)/\rho_B \text{ or,}$$

$$T{:}B = V_P\rho_B/(1\text{-}H_B) \quad [3]$$

That is, the dimensionless T:B ratio as defined here is proportional to the specific plasma distribution volume of an organ scaled by a factor that depends on the hematocrit and whole blood density of that sample. Since there is only one whole blood sample for each animal, the same proportionality factor is applied to every tissue in that animal and the relative magnitudes of T:B ratios across organs in that animal are determined without bias. On the other hand, this proportionality factor can vary across animals, primarily through variations in (here, arterial) hematocrit, so that T:B ratios across differnt animals will also vary. However, in the present study, animal ages and weights were similar across the study population so that variations in this factor likely constitute a relatively small source of error in population estimates of T:B ratios. Finally, if typical values for blood density (1.06 g/ml) and hematocrit (0.45) are inserted into Eqn. 3, T:B ratios as defined here will overestimate the true specific organ plasma distribution volume by about a factor of 2. These considerations should be borne in mind when interpreting the results portayed Figures 4C and 6.

References

1. Todica A, Brunner S, Boning G, Lehner S, Nekolla SG, Wildgruber M, et al. [^{68}Ga]-albumin-PET in the monitoring of left ventricular function in murine models of ischemic and dilated cardiomyopathy: comparison with cardiac MRI. Mol Imaging Biol 2013;15:441–449. [PubMed: 23408338]

2. Abidov A, Germano G, Hachamovitch R, and Berman DS. Gated SPECT in assessment of regional and global left ventricular function: major tool of modern nuclear imaging. J Nucl Cardiol 2006;13:261–279. [PubMed: 16580963]
3. Ito H, Kanno I, and Fukuda H. Human cerebral circulation: positron emission tomography studies. Ann Nucl Med 2005;19:65–74. [PubMed: 15909484]
4. Middleton ML and Strober MD. Planar scintigraphic imaging of the gastrointestinal tract in clinical practice. Semin Nucl Med 2012;42:33–40. [PubMed: 22117811]
5. Kumar V and Boddeti DK. ^{68}Ga-radiopharmaceuticals for PET imaging of infection and inflammation. Recent Results Cancer Res 2013;194:189–219. [PubMed: 22918761]
6. Schuster DP. The evaluation of lung function with PET. Semin Nucl Med 1998;28:341–51. [PubMed: 9800239]
7. Grady E Gastrointestinal Bleeding Scintigraphy in the Early 21st Century. J Nucl Med 2016;57:252–259. [PubMed: 26678616]
8. Yates PA, Villemagne VL, Ellis KA, Desmond PM, Masters CL, and Rowe CC. Cerebral microbleeds: a review of clinical, genetic, and neuroimaging associations. Front Neurol 2014;4:205. [PubMed: 24432010]
9. Niu G, Lang L, Kiesewetter DO, Ma Y, Sun Z, Guo N, et al. In Vivo Labeling of Serum Albumin for PET. J Nucl Med 2014;55:1150–1156. [PubMed: 24842890]
10. Wang WY, Tang YD, Yang M, Cui C, Mu M, Qian J, et al. Free triiodothyronine level indicates the degree of myocardial injury in patients with acute ST-elevation myocardial infarction. Chin Med J 2013;126:3926–3929. [PubMed: 24157158]
11. Russell RR, 3rd and Zaret BL Nuclear cardiology: present and future. Curr Probl Cardiol 2006;31:557–629. [PubMed: 16935694]
12. Chen J, Boogers MJ, Bax JJ, Soman P, and Garcia EV. The use of nuclear imaging for cardiac resynchronization therapy. Curr Cardiol Rep 2010;12:185–191. [PubMed: 20425175]
13. de Geus-Oei LF, Mavinkurve-Groothuis AM, Bellersen L, Gotthardt M, Oyen WJ, Kapusta L, et al. Scintigraphic techniques for early detection of cancer treatment-induced cardiotoxicity. J Nucl Med Technol 2013;41:170–181. [PubMed: 23929800]
14. Russell RR, Alexander J, Jain D, Poornima IG, Srivastava AV, Storozynsky E, et al. The role and clinical effectiveness of multimodality imaging in the management of cardiac complications of cancer and cancer therapy. J Nucl Cardiol 2016;23:856–884. [PubMed: 27251147]
15. Herman LW, Fischman AJ, Tompkins RG, Hanson RN, Byon C, Strauss HW, et al. The use of pentafluorophenyl derivatives for the ^{18}F labelling of proteins. Nucl Med Biol 1994;21:1005–1010. [PubMed: 9234356]
16. Wester H-J, Hamacher K, and Stocklin G. A comparative study of N.C.A. Fluorine-18 labeling of proteins via acylation and photochemical conjugation. Nucl Med Biol 1996;23:365–372. [PubMed: 8782249]
17. Kilbourn MR, Dence CS, Welch MJ, and Mathias CJ. Fluorine-18 Labeling of Proteins. J Nucl Med 1987;28:462–470. [PubMed: 3494825]
18. Chang YS, Jeong JM, Lee Y-S, Kim HW, Rai GB, Lee SJ, et al. Preparation of ^{18}F-Human Serum Albumin: A Simple and Efficient Protein Labeling Method with ^{18}F Using a Hydrazone-Formation Method. Bioconjug Chem 2005;16:1329–1333. [PubMed: 16173815]
19. Ramenda T, Kniess T, Bergmann R, Steinbach J, and Wuest F. Radiolabelling of proteins with fluorine-18 via click chemistry. Chem Commun 2009:7521–7523.
20. Kostikov AP, Chin J, Orchowski K, Niedermoser S, Kovacevic MM, Aliaga A, et al. Oxalic acid supported Si-^{18}F-radiofluorination: one-step radiosynthesis of N-succinimidyl 3-(di-tert-butyl[^{18}F]fluorosilyl)benzoate ([^{18}F]SiFB) for protein labeling. Bioconjug Chem 2012;23:106–114. [PubMed: 22148255]
21. Wängler B, Quandt G, Iovkova L, Schirrmacher E, Wangler C, Boening G, et al. Kit-Like ^{18}F-Labeling of Proteins: Synthesis of 4-(Di-tert-butyl[^{18}F]fluorosilyl)benzenethiol (Si[^{18}F]FA-SH) Labeled Rat Serum Albumin for Blood Pool Imaging with PET. Bioconjug Chem 2009;20:317–321. [PubMed: 19132825]

22. Kang CM, Kim H, Koo HJ, Park JW, An GI, Choi JY, et al. Catabolism of ^{64}Cu and Cy5.5-labeled human serum albumin in a tumor xenograft model. Amino Acids 2016;48:1667–1675. [PubMed: 27098932]
23. Basuli F, Li C, Xu B, Williams M, Wong K, Coble VL, et al. Synthesis of Fluorine-18 Radiolabeled Serum Albumins for PET Blood Pool Imaging. Nucl Med Biol 2015;42:219–225. [PubMed: 25533724]
24. Olberg DE, Arukwe JM, Grace D, Hjelstuen OK, Solbakken M, Kindberg GM, et al. One Step Radiosynthesis of 6-[^{18}F]Fluoronicotinic Acid 2,3,5,6-Tetrafluorophenyl Ester ([^{18}F]F-Py-TFP): A New Prosthetic Group for Efficient Labeling of Biomolecules with Fluorine-18. J Med Chem 2010;53:1732–1740. [PubMed: 20088512]
25. McBride WJ, Sharkey RM, Karacay H, D'Souza CA, Rossi EA, Laverman P, et al. A Novel Method of ^{18}F Radiolabeling for PET. J Nucl Med 2009;50:991–998. [PubMed: 19443594]
26. Shetty D, Choi SY, Jeong JM, Lee JY, Hoigebazar L, Lee Y-S, et al. Stable aluminium fluoride chelates with triazacyclononane derivatives proved by X-ray crystallography and ^{18}F-labeling study. Chem Commun 2011;47:9732–9734.
27. McBride WJ, D'Souza CA, Sharkey RM, Karacay H, Rossi EA, Chang C-H, et al. Improved ^{18}F Labeling of Peptides with a Fluoride-Aluminum-Chelate Complex. Bioconjug Chem 2010;21:1331–1340. [PubMed: 20540570]
28. McBride WJ, D'Souza CA, Sharkey RM, and Goldenberg DM. The radiolabeling of proteins by the [^{18}F]AlF method. Appl Radiat Isot 2012;70:200–204. [PubMed: 21890371]
29. Chen Q, Meng X, McQuade P, Rubins D, Lin S-A, Zeng Z, et al. Synthesis and Preclinical Evaluation of Folate-NOTA-Al^{18}F for PET Imaging of Folate-Receptor-Positive Tumors. Mol Pharm 2016;13:1520–1527. [PubMed: 27054811]
30. Poschenrieder A, Osl T, Schottelius M, Hoffmann F, Wirtz M, Schwaiger M, et al. First ^{18}F-Labeled Pentixafor-Based Imaging Agent for PET Imaging of CXCR4 ExpressionIn Vivo. Tomography 2016;2:85–93. [PubMed: 30042959]
31. Cleeren F, Lecina J, Ahamed M, Raes G, Devoogdt N, Caveliers V, et al. Al^{18}F-Labeling Of Heat-Sensitive Biomolecules for Positron Emission Tomography Imaging. Theranostics 2017; 7:2924–2939. [PubMed: 28824726]
32. Da Pieve C, Allott L, Martins CD, Vardon A, Ciobota DM, Kramer-Marek G, et al. Efficient [^{18}F]AlF Radiolabeling of ZHER3:8698 Affibody Molecule for Imaging of HER3 Positive Tumors. Bioconjug Chem 2016;27:1839–1849. [PubMed: 27357023]
33. Cleeren F, Lecina J, Billaud EMF, Ahamed M, Verbruggen A, and Bormans GM. New Chelators for Low Temperature Al^{18}F-Labeling of Biomolecules. Bioconjug Chem 2016;27:790–798. [PubMed: 26837664]
34. Cleeren F, Lecina J, Ahamed M, Raes G, Devoogdt N, Caveliers V, et al. Al^{18}F-Labeling Of Heat-Sensitive Biomolecules for Positron Emission Tomography Imaging. Theranostics 2017;7:2924–2939. [PubMed: 28824726]
35. Wang Y, Seidel J, Tsui BMW, Vaquero JJ, and Pomper MG. Performance Evaluation of the GE Healthcare eXplore VISTA Dual-Ring Small-Animal PET Scanner. J Nucl Med 2006;47:1891–1900. [PubMed: 17079824]
36. Herraiz JL, España S, Vaquero JJ, Desco M, and Udías JM. FIRST: Fast Iterative Reconstruction Software for (PET) tomography. Phys Med Biol 2006;51:4547. [PubMed: 16953042]
37. Glaser M, Iveson P, Hoppmann S, Indrevoll B, Wilson A, Arukwe J, et al. Three methods for ^{18}F labeling of the HER2-binding affibody molecule Z(HER2:2891) including preclinical assessment. J Nucl Med 2013;54:1981–1988. [PubMed: 24115530]
38. Lockett MR, Phillips MF, Jarecki JL, Peelen D, and Smith LM. A Tetrafluorophenyl Activated Ester Self-Assembled Monolayer for the Immobilization of Amine-Modified Oligonucleotides. Langmuir 2008;24:69–75. [PubMed: 18047381]
39. Altman PL. Blood and other body fluids: Federation of American Societies for Experimental Biology,1961.
40. Hoffend J, Mier W, Schuhmacher J, Schmidt K, Dimitrakopoulou-Strauss A, Strauss LG, et al. Gallium-68-DOTA-albumin as a PET blood-pool marker: experimental evaluation in vivo. Nucl Med Biol 2005;32:287–292. [PubMed: 15820764]

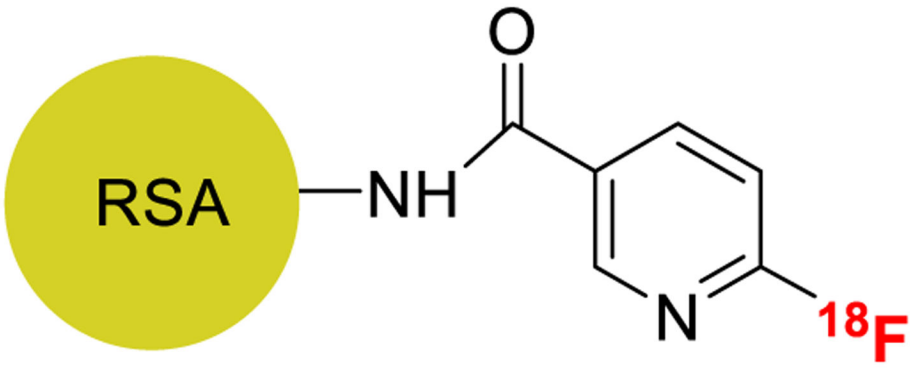

Figure 1.
Structure of [^{18}F]F-NE-RSA

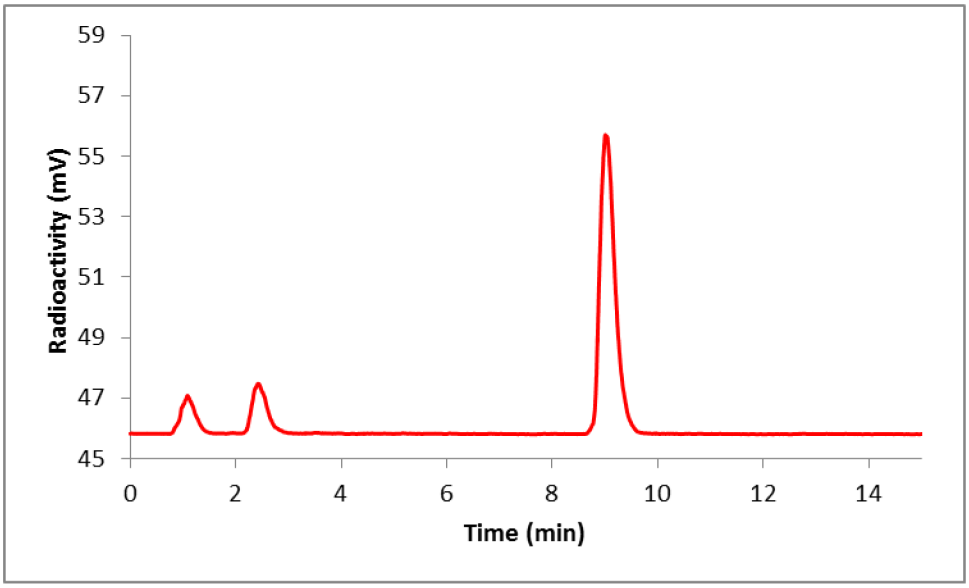

Figure 2.
Radio-HPLC profile of crude reaction mixture of [^{18}F]AlF-NODA-Bz-TFPE. HPLC conditions: method B.

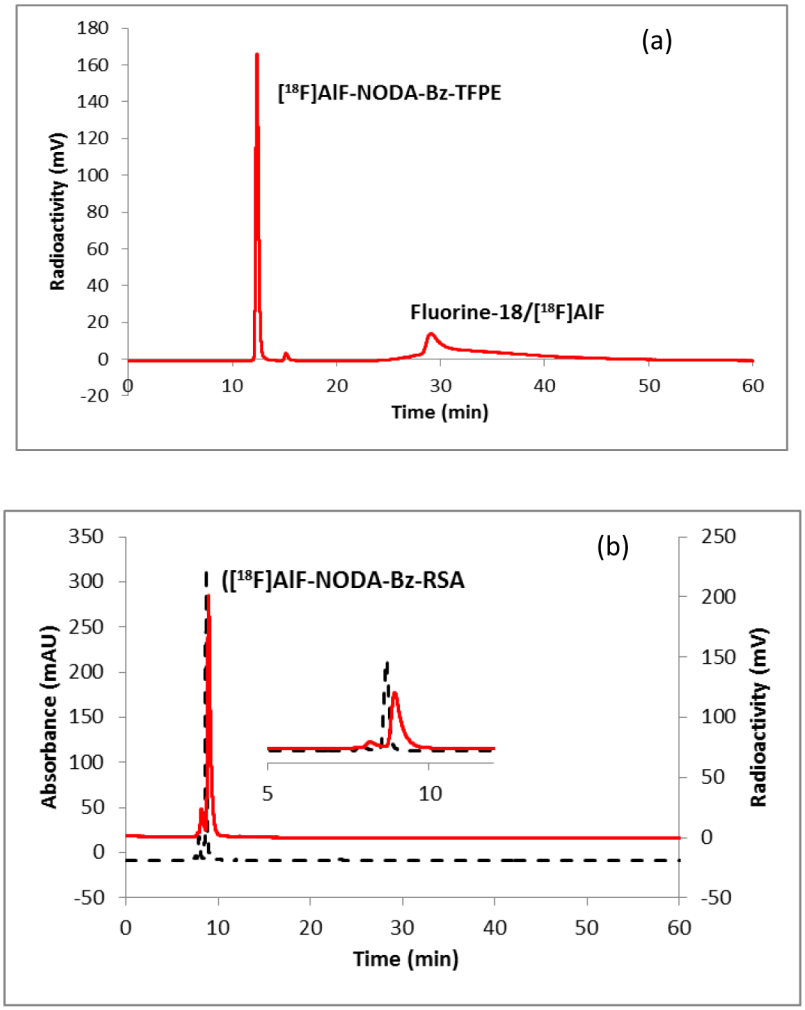

Figure 3.

HPLC chromatogram of (a) [^{18}F]AlF-NODA-Bz-TFPE, reaction mixture; (b) [^{18}F]AlF-NODA-Bz-RSA. HPLC condition: method C; Solid line, in-line radio detector; dotted line, UV detector at 254 nm

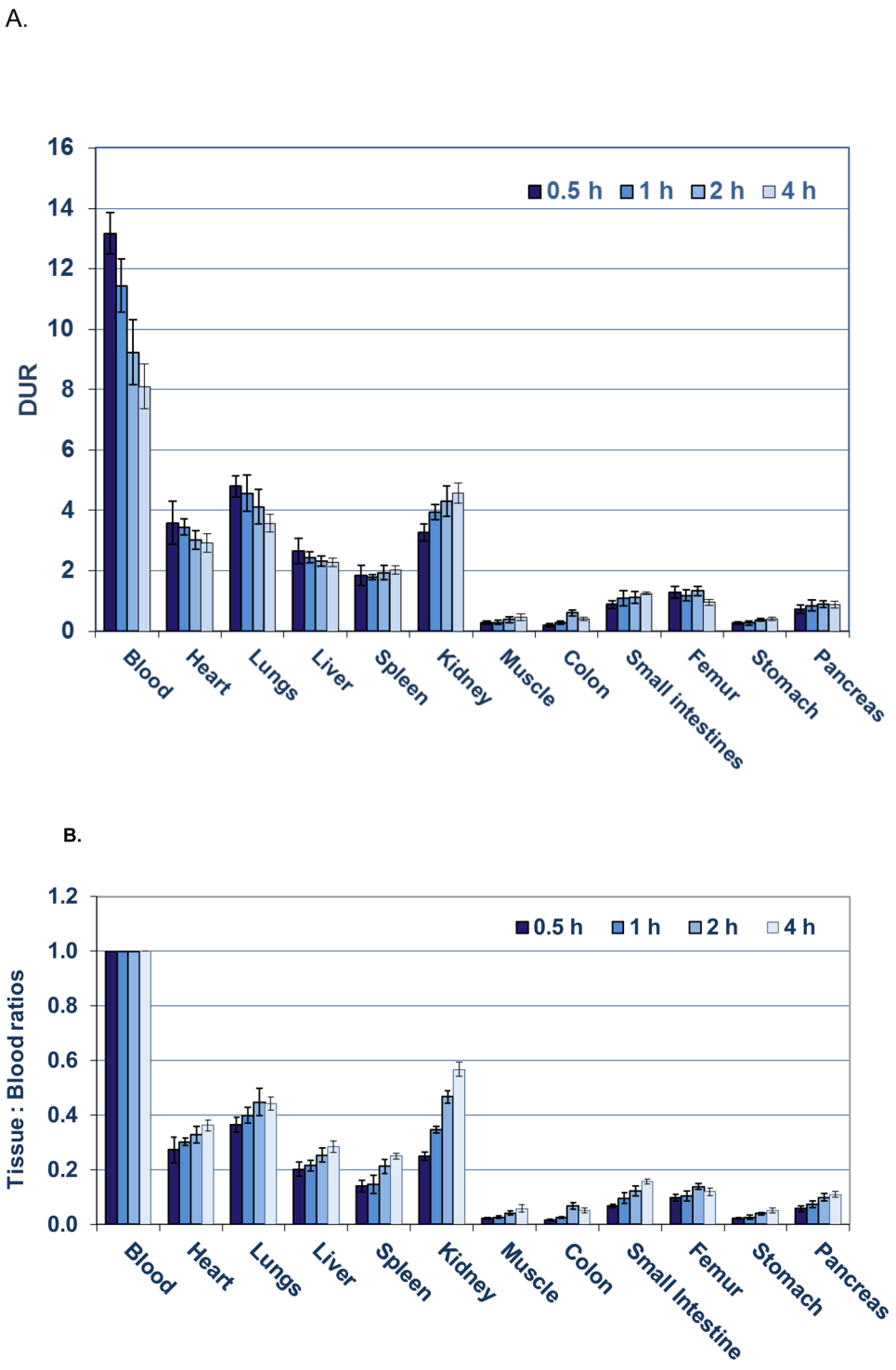

Figure 4.

A) Biodistribution of [^{18}F]AlF-NODA-Bz-RSA in rats from 0.5 to 4 h. Each bar represents the mean DUR ± SD of [^{18}F]AlF-NODA-Bz-RSA (n =5).

B) Tissue to blood ratios (T:B) of [^{18}F]AlF-NODA-Bz-RSA from 0.5 to 4 h. Bars represent mean T:B ± SD (n= 5).

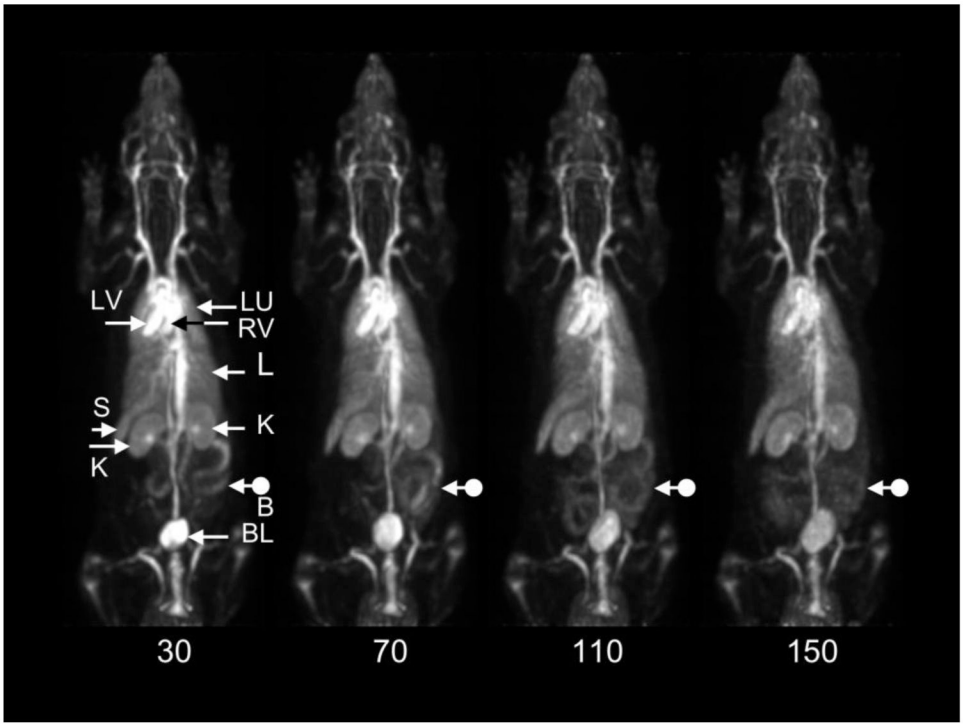

Figure 5.

Decay-corrected, consecutive whole-body posterior view maximum intensity projection images of a 170 g rat following injection of 580 μCi (21.5 MBq) of [^{18}F]AlF-NODA-Bz-RSA. Data were acquired for 10 minutes in each of four bed positions starting at the head in each whole-body (WB) scan. The start time of each WB scan relative to the time of injection is shown below each scan. LV: left ventricle; RV: right ventricle; LU: lungs; L: liver; K: kidneys; S: spleen; BL: bladder; B: bowel. Note changing distribution of bowel activity (dot arrows) with time.

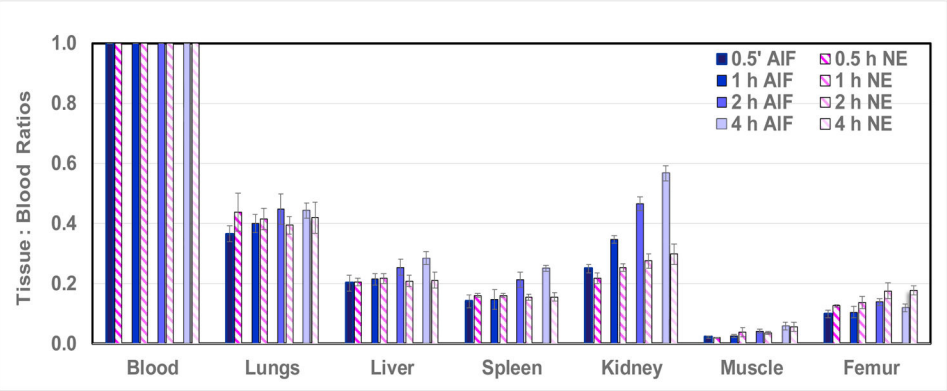

Figure 6.

Tissue to blood ratios (T:B) from 0.5 to 4 h of [^{18}F]RSA-AlF (prepared using the AlF method) compared to [^{18}F]RSA-NE (prepared using the nicotinic ester method). Bars represent mean T:B ± SD (n= 5).

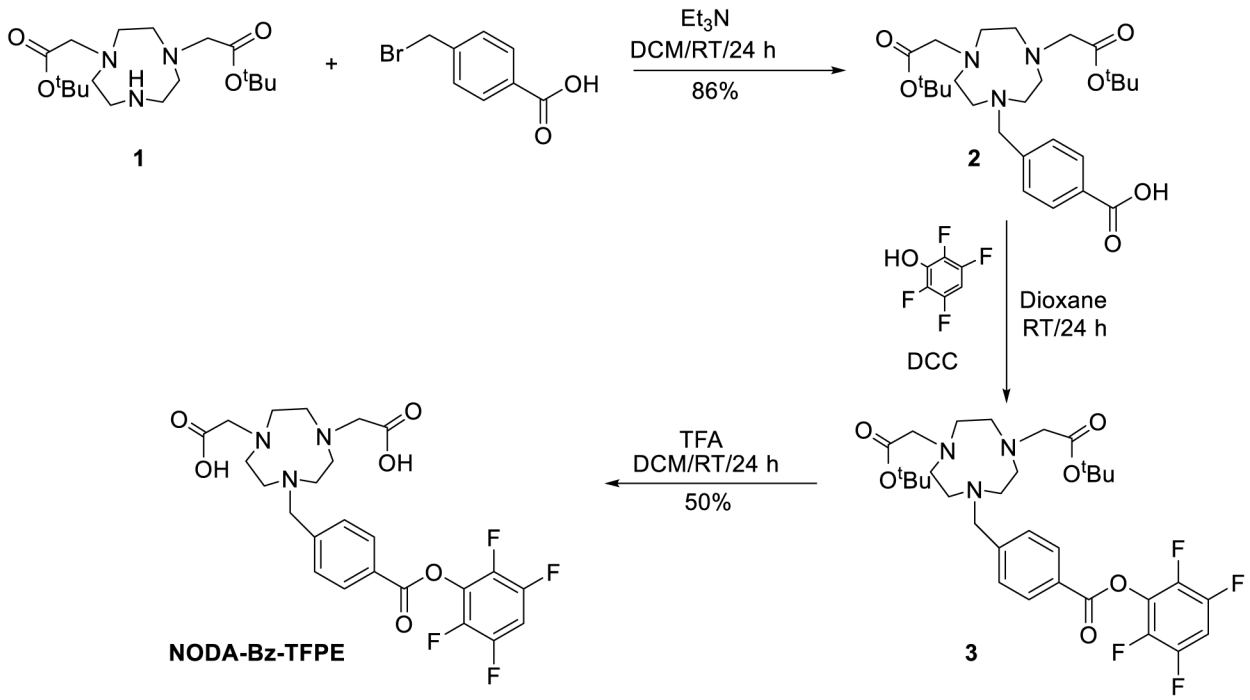

Scheme 1.
Preparation of NODA-Bz-TFPE ligand

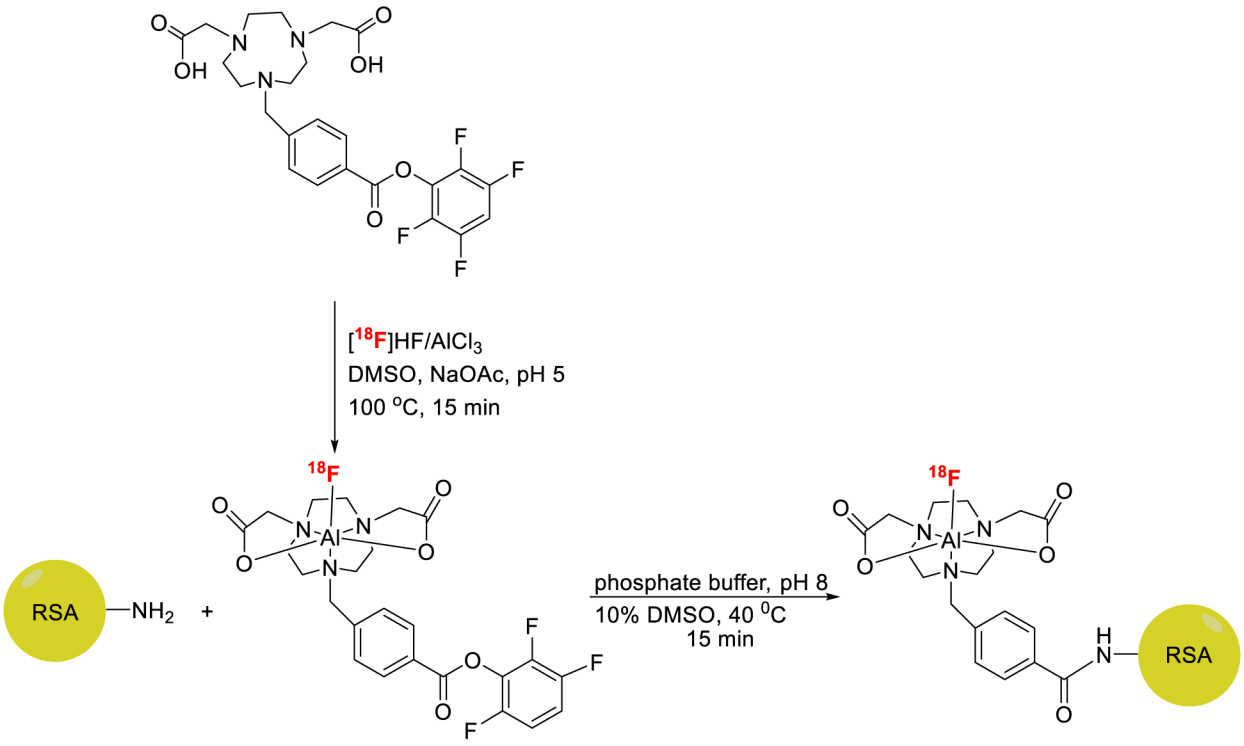

Scheme 2.
Preparation of [^{18}F]AlF-NODA-Bz-TFPE and [^{18}F]RSA-AlF

Table 1.

Increases in Al[^{18}F]F-NODA-Bz-RSA tissue to blood ratios (T:B) with time in awake rats.

	PERCENT INCREASE (T:B)		
	0.5-1h	***0.5-2h***	***0.5-4h***
HEART	*10.0*	*17.2*	*33.0**
LUNGS	*8.6*	*18.4**	*21.2***
LIVER	*6.0*	*20.5**	*41.0***
SPLEEN	*3.7*	*33.8***	*78.1***
KIDNEY	*28.0**	*46 6****	*127.9****
MUSCLE	*16.4*	*47.9****	*169.9***
COLON	*35.4*	*76.6****	*219.5****
SMALL INTESTINE	*29.6**	*44.8****	*76.6****
FEMUR	*5.6*	*28.8***	*44.8**
STOMACH	*16.2*	*45.2****	*28.8****
PANCREAS	*23.6*	*42.52****	*45.2****

* $P < 0.05$;

** $P < 0.01$;

*** $P < 0.001$ (n = 5 per group, Welch's T test), represents a significant increase in T:B ratio compared to 0.5 h.